Poly-γ-Glutamic acid Hydrogels as Electrolyte for Poly(3,4-ethylenedioxythiophene) Based Supercapacitors

Maria M. Pérez-Madrigal,[1,2,*] Miquel G. Edo,[1,2] Angélica Díaz,[1,2] Jordi Puiggalí[1,2] and Carlos Alemán[1,2,*]

[1] *Departament d'Enginyeria Química, ETSEIB, Universitat Politècnica de Catalunya, Avda. Diagonal 647, Barcelona E-08028, Spain*

[2] *Center for Research in Nano-Engineering, Universitat Politècnica de Catalunya, Campus Sud, Edifici C', C/Pasqual i Vila s/n, Barcelona E-08028, Spain*

[*] **m.mar.perez@upc.edu** and **carlos.aleman@upc.edu**

ABSTRACT

Biosynthetic poly-γ-glutamic acid (γ-PGA) has been used to produce hydrogels using cystamine as cross-linker and 1-[3-(dimethylamino)propyl]-3-ethylcarbodiimide methiodide (EDC methiodide) as condensing agent. Eight different hydrogels with different properties were formulated by varying both the molecular weight of γ-PGA and the γ-PGA/EDC/cystamine ratio, and subsequently characterized. The most appropriate γ-PGA hydrogel was selected to perform as solid electrolytic medium in organic electrochemical supercapacitors (OESCs) using poly(3,4-ethylenedioxythiophene) (PEDOT) electrodes based on their mechanical behaviour (consistency and robustness to hold the PEDOT electrodes), morphology, and influence on the electrochemical response of the organic electrode (*i.e.* specific capacitance, and both maximum energy and power densities values). Hence, PEDOT/γ-PGA energy storage devices fabricated using the most adequate hydrogel formulation displayed a supercapacitor response of 168 F/g and a capacitance retention of 81%. Moreover, after evaluating the maximum energy and power densities (Ragone plot), cyclability, long-term stability, leakage-current, and self-discharging response of PEDOT/γ-PGA OESC devices, results allow us to highlight the merits and great potential of γ-PGA hydrogels as sustainable ion-conductive electrolytes for environmentally friendly energy storage technologies.

INTRODUCTION

Our daily activities have become dependent on the available energy supply. Indeed, portable energy storage devices have become essential, not only for operating laptops and smart cell phones, but also for other electronic and electrical systems used in motor vehicles, satellites, sensors, or medical and military equipment. Among other features, these applications require energy storage devices to be cost-affordable, light-weight, durable (long-term stability) and, if possible, sustainable by using eco-friendly materials.

Although electrolytic/ceramic batteries and capacitors are both used for energy storage applications, these devices differ in the power and energy densities they can provide. Thus, batteries are characterized by high energy density values (10-100 Wh/kg), while capacitors display high power density values (*i.e.* they can release the stored energy much faster).[1] In low-energy applications (*e.g.* motor starting, signal processing and sensing) or when fast pulsed power supply is needed (*e.g.* electromagnetic forming, Marx generators, pulsed lasers, and particle accelerators, among others), capacitors offer a series of advantages, such as cost-effectiveness, faster charging-discharging times, and long-lasting cycling stability.

Electrochemical supercapacitors (ESCs) have emerged as promising energy storage devices displaying higher energy values (*i.e.* 1-10 Wh/kg for carbon ESCs) than conventional capacitors (*i.e.* < 0.1 Wh/kg), evidencing a potential future use in large-scale high-energy applications.[2] In ESCs, the electric double-layers formed at the electrode-electrolyte interface (*i.e.* Helmholtz and diffuse layers) contribute to the magnitude of the capacitance, which strongly depends on the electrode surface.[3] In order to increase the capacitance, faradic charge transfer reactions are frequently employed by applying electrochemically active materials, such as metal oxide materials

or conducting polymers (CPs). Similarly to metal oxides, CPs display competitive capacitance values (from 60 up to 1000 F/g, depending on the CP) with a potential range of 0.8 V but offering advantages in cost, processability and light-weight. On the other hand, the charge storage mechanism of CPs requires ions to be intercalated into the polymeric 3D network, which causes chemical degradation and swelling, and thus a possible reduction in the cycle life of the electrode.[3] For example, poly(3,4-ethylenedioxythiophene) (PEDOT) has been reported as an adequate electrode in organic ESCs (OESCs).[4-8] In addition to showing capacitance values in the range between 60 and 250 F/g, this electrochemically active material is electrostable and biocompatible.[9-12]

Recent research in OESCs has been focused on improving their energy density, which is the limiting specification that restricts their application in large-scale energy storage systems, by either increasing the capacitance of the device, the operation voltage window, or both. The approaches followed to reach such purpose include: nanostructuring and increasing the electrode porosity,[13-15] designing electrodes with a gel-like morphology,[16] or combining the CP with metal oxides (*e.g.* MnO_2 or V_2O_5),[17,18] carbon nanotubes,[19] graphene oxide,[20] or redox biopolymers (*e.g.* lignin).[21]

Nevertheless, even though pseudocapacitance depends primarily on the electrode conductivity, porosity, size, and surface shape, it is also affected by the ion movement speed in the electrolyte.[3] Dopant ions transport represents a critical factor, especially for thick electrodes (> 100 μm), since it determines the fraction of electrode accessible electrochemically and, thus, contributing to the pseudocapaticance of the system.[22] Bearing this idea in mind, new electrolytes, such as ionic liquids[23,24] or gels[25], have been used to provide high potential stability windows and improve the electrochemical stability of the electrodes.

In addition, due to the global concern regarding sustainable technology, efforts are being made to replace organic solvents usually used in electrolytes for ESCs devices by aqueous solutions.[26] Besides, when the electrolyte is presented in solid form (*i.e.* solid electrolyte, SE) further advantages are obtained: compactness, reliability, reduced leakage risk, flexibility, and easy of handling.[27] Very recently, Armelin *et al*. reviewed the use of biohydrogels for supercapacitor applications.[28] These materials, which can be extracted directly or eventually synthesized/recycled from biomass and renewable sources, represent the next stage towards a more sustainable energy storage technology. Within this context, we prepared and evaluated the supercapacitor performance of OESC devices using PEDOT as electrodes and four different biohydrogels as SE (*i.e.* sodium alginate, κ-carrageenan, gelatin, and chitosan).[25] In order to exploit at maximum the pseudocapacitance of PEDOT electrodes, these SEs were expected to present, not only mechanical robustness to keep the electrodes at their positions, but also an open porous structure able to favour ion movement and transfer. We found that κ-carrageenan was the most suitable biohydrogel to perform as SE electrolyte due to the appropriate combination of properties: mechanical integrity, lack of water leaking, and structural suitability to favour the electrochemical response of PEDOT.[25] Nevertheless, it should be noted that the pores in those biohydrogels were based on physical cross-links (*i.e.* polymeric chains were cross-linked by monovalent or divalent metallic ions), hindering the control/tuning of their structural characteristics.

Therefore, herein, we explore the use of hydrogels based on poly-*γ*-glutamic acid (*γ*-PGA) as SE in OESC devices. *γ*-PGA is a poly(*γ*-peptide) derived from glutamic acid (Glu), in which peptide bonds involve the *γ*-carboxyl group and *α*-amino groups (Scheme 1). This compound is naturally synthetized as a slime layer by a variety of members of the genus *Bacillus.*[29] For instance, the molecular weight of *γ*-PGA produced

by *Bacillus subtilis* isolated from "chungkookjang", a traditional Korean fermented soybean food,[30] is much higher than that obtained using *Bacillus subtilis natto*, which allows its functional application in cosmetics, medicine, and industrial products (*e.g.* water absorption agents, moisturizing agents, thickening agents, absorption enhancers of minerals, sustained release drug delivery systems, and biodegradable agglomerated detergents).[31] In addition, in its free-acid form, *γ*-PGA can be chemically cross-linked producing biohydrogels.[32-34] Most importantly, the structure and content of the cross-linker agent, regulates the cross-linking density, pore size, water absorption, and degradation profile of the resulting *γ*-PGA hydrogels.[32-34]

In this work, up to eight *γ*-PGA hydrogel formulations have been prepared by varying the molecular weight of the biopolymer and the cross-linking degree. These parameters affected the morphology, swelling ratio, thermal properties, and mechanical integrity of the hydrogels. After selecting those *γ*-PGA hydrogels with the most appropriate properties to perform as electrolytic medium in OESC devices, the electrochemical response of PEDOT electrodes has been evaluated in terms of specific capacitance (*SC*), maximum energy density (E_{max}) and power density (P_{max}). Finally, features directly related to the application of the system, such as cyclability, long-term stability, and the lighting of a LED bulb, have been further examined for the optimum PEDOT/ *γ*-PGA OESC.

EXPERIMENTAL SECTION

Preparation of PEDOT/γ-PGA OESC devices. Specific experimental details for the synthesis of PEDOT films and *γ*-PGA hydrogels are provided in Supporting Information. As a general procedure, *γ*-PGA hydrogels used as SE were prepared 24 hours before testing and without applying the washing step. Thus, the response of

PEDOT is not hindered by the presence of 1-[3-(dimethylamino)propyl]-3-ethylcarbodiimide methiodide (EDC methiodine) or cystamine but by the lack of electrolyte, $NaHCO_3$. Therefore, *ca.* 1.4 mL of the reaction solution was placed into the wells of a 24-well plate and let to gel at room temperature. Before the electrochemical characterization, PEDOT films electropolymerized onto SS sheets were carefully introduced into the *γ*-PGA hydrogel at a distance of 1 cm and fixed with tape to prevent movement during testing (Figure S1).

Characterization. Details on all physical and chemical characterization measures are provided in the Supporting Information with exception of the electrochemical characterization that is described here. Although the three-electrode electrochemical cell configuration is adequate for a fast screening of the electrode material, the two-electrode configuration confirms the supercapacitor performance under specific working conditions since the response of the whole cell is under investigation. Accordingly, the electrochemical response of PEDOT electrodes was firstly studied using three different *γ*-PGA hydrogels as SE (compositions LPGGA-2, LPGGA-4 and HPGGA-6 in Table S1) in a two-electrode configuration (PEDOT/SS = WE/S; PEDOT/SS = CE/RE).

As defined by Stoller and Ruoff,[35] the *SC* (F/g) is the capacitance per unit of mass for one electrode, and can be expressed as

$$SC = 4 \times \frac{C}{m} \qquad (2)$$

where *C* is the measured capacitance for the two-electrode cell and *m* the total mass of the active material in both electrodes (*i.e.* 0.8226 mg). The multiplier 4 adjusts the capacitance of the cell and the combined mass of the two electrodes to the capacitance and mass of a single electrode.

Galvanostatic charge/discharge (GCD) evaluation is the most commonly used procedure to determine the cell capacitance (*C*, F) of a pseudocapacitor:

$$C = \frac{I}{\left(\frac{dV}{dt}\right)} \qquad (3)$$

where *I* is the discharging current applied to the device, and *dV/dt* should be calculated as $(V_{max} - ½ \cdot V_{max})/(t_2 - t_1)$, where V_{max} corresponds to the highest voltage in the GCD curve after the voltage drop (V_{drop}) at the beginning of the discharging process.[35]

Consequently, GCD curves (5 cycles) between 0.0 and 0.8 V were run at different current densities (*i.e.* charge and discharge rates are specified in units of current per electrode mass): 0.30, 0.44, 0.61, 1.22, 2.43 and 4.86 A/g that corresponded to 0.125, 0.18, 0.25, 0.5, 1 and 2 mA, respectively. Besides, the coulombic efficiency (η, %) was evaluated as the ratio between the discharging and charging times for the electrochemical window between 0 V and 0.8 V:

$$\eta = \frac{t_d}{t_c} \qquad (4)$$

Finally, cyclic voltammetry (CV) measurements can also provide information regarding the cell capacitance (*C*, F) of a system by applying Eq 3. In this case, *I* corresponds to the average current during discharging (*i.e.* PEDOT reduction from 0.7082 to 0.1012 V), while *dV/dt* is the scan rate. Specifically, for PEDOT/γ-PGA OESC devices, CV curves (5 cycles) were recorded from 0 V to 0.8 V at several scan rates: 10, 25, 50, 75, 100, 150 and 200 mV/s.

All electrochemical experiments (GCD and CV curves) were run in triplicate, and the results presented are the average data (mean ± SD). In addition, $NaHCO_3$ solution (0.5 M) was tested as control electrolyte.

After selecting the most appropriate γ-PGA hydrogel system as electrolyte, the cycling stability of the corresponding PEDOT/γ-PGA OESC device was tested by two approaches. Firstly, the system was submitted to 2,000 GCD cycles at a current density of 1.22 A/g from 0 V to 0.8 V, which corresponds to t_c and t_d values of approximately 40-60 seconds. Secondly, 1,000 CV cycles were run from 0 V to 0.8 V at 50 mV/s. The time-dependence evolution of the supercapacitor response was determined after 1 week by repeating the GCD test (2,000 cycles) for the same sample. From the CV curves, the electrostability of PEDOT electrodes was quantified as the loss of electroactivity (LEA; in %):

$$LEA = \frac{\Delta Q}{Q_2} = \frac{Q_i - Q_2}{Q_2} \quad (5)$$

where ΔQ is the difference between the oxidation charge (in C) of the second (Q_2) and the evaluated oxidation-reduction cycle (Q_i).

Moreover, the leakage current (LC) and self-discharging (SD) response of PEDOT/γ-PGA devices was evaluated by applying methods previously described.[36] For the former, after charging the device to 0.8 V at 0.25 mA (*i.e.* 0.61 A/g), it was kept at 0.8 V for 5-10 min while recording the current. For the latter, PEDOT/γ-PGA devices were charged to 0.8 V at 0.25 mA, kept at 1E-11 mA for 10 min (self-discharging). After that time, the device was discharged to 0 V at -1 mA. Data was obtained from three different devices.

Finally, the E_{max} (Wh/kg), which is the amount of energy stored per unit of mass, and P_{max} (W/kg), which describes the speed at which the energy stored can be delivered, can be calculated by applying the following equations:[37]

$$E_{max} = \frac{1}{2} \times V_{max}^2 \times SC \quad (6)$$

$$P_{\max} = \frac{1}{4m} \times \frac{V_{\max}^2}{R_i} \quad (7)$$

$$R_i = \frac{V_{drop}}{2 \times I_{discharge}} \quad (8)$$

where V_{max} corresponds to the highest voltage in the GCD curve after V_{drop}, m is the total mass of the active material in one electrode (*i.e.* 0.4113 mg) and R_i is the internal resistance.

RESULTS AND DISCUSSION

Preparation of PEDOT electrodes

This work focuses on the role of γ-PGA hydrogels as green and aqueous-based SE for OESC devices. Hence, PEDOT electrodes were prepared by applying an optimized procedure previously reported in the literature:[25] chronoamperometry (CA) under a potential of 1.25 V and a polymerization charge of 0.5 C/cm^2. The resulting PEDOT films exhibited a thickness of 4.12 ± 0.83 μm, an electrical conductivity of 33.2 ± 4.1 S/cm, and a mass of 0.4113 ± 0.057 mg.

Regarding the morphology, PEDOT films display a sponge-like porous structure with a continuous open network and void spaces (Figure S2a-b). Besides, PEDOT chain entanglements form aggregates of varying size and height (between 1 and 5 μm) that are distributed throughout the surface resulting in Rq values of 633 ± 22 nm for 10 × 10 μm^2 areas (Figures S2c-d). Such matrix features favour fast ion and electron transport during electrochemical redox processes, and thus allow for high charge storage and pseudocapacitance of the OESC device.

Preparation of γ-PGA hydrogels and their pre-selection as electrolyte for OESC devices

In addition to facilitate an adequate ion movement towards the electrode, a superior electrolyte performance is based on optimized working voltages, non-toxicity, low corrosion, and safety.[3] Accordingly, γ-PGA hydrogels seem an excellent option to be applied as SE in OESCs devices. In this work, γ-PGA hydrogels were produced by adapting the procedure described by Matsusaki *et al.*[38] that uses cystamine as cross-linker (Scheme 1).

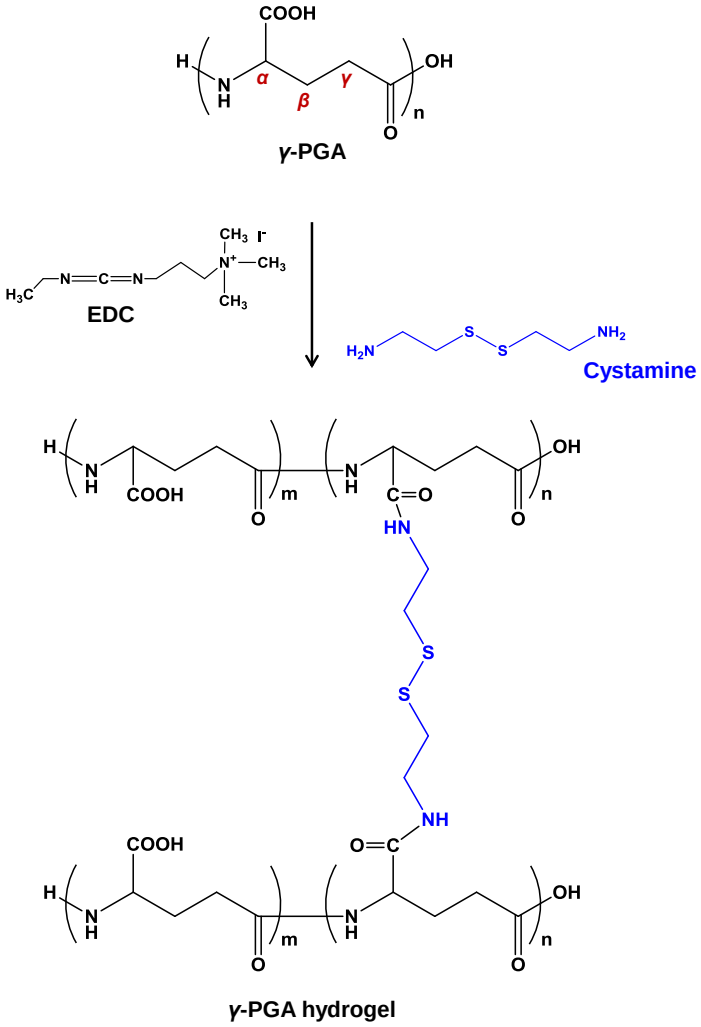

Scheme 1. Synthetic route for the preparation of γ-PGA hydrogels using cystamine as cross-linker.

Table S1 summarizes the different γ-PGA hydrogels prepared by varying the concentration of the compounds involved in the condensation reaction: γ-PGA, EDC, and cystamine. The prepared hydrogels have been labelled LPGGA-# and HPGGA-# for samples derived from low and high molecular weight γ-PGA, respectively, # being a number used to identify the cystamine and EDC concentrations ([Cys] and [EDC], respectively).

The pre-selection of the γ-PGA hydrogels for their use as electrolyte in OESC devices was performed according to the following rational:

- The mechanical integrity of suitable γ-PGA hydrogels must be enough to keep the PEDOT electrodes at their positions. For this purpose, evaluation of the mechanical properties has been performed by visual inspection.
- The porosity of suitable γ-PGA hydrogels must be adequate enough to maximize the pseudocapacitance of PEDOT electrodes by promoting ion movement at the electrode-electolyte interface. The morphology of the prepared hydrogels was evaluated by scanning electron microscopy (SEM).

The swelling ratio (SR, %) of the resulting γ-PGA hydrogels, which is a good indicative of their cross-linking degree, decreases with increasing content of cystamine (Table S1). Besides, hydrogels prepared with low M_w γ-PGA exhibit lower cross-linking than those prepared with high M_w γ-PGA. The mechanical stability of γ-PGA hydrogels was found to improve with the cystamine concentration (*i.e.* cross-linking density). For instance, the mechanical integrity of LPGGA-1, a transparent hydrogel with low cross-linking, was poor (Figure S3a) while, in opposition, HPGGA-6 was a robust, opaque and compact hydrogel (Figure S3b).

SEs are required to present an open porous structure. SEM micrographs of γ-PGA hydrogels that displayed a stable mechanical integrity (*i.e.* LPGGA-2, -4, and -5; and all

three HPPGA-#) are displayed in Figures 1 and S4. Samples exhibited pore sizes in the range between 1.4 and 25 μm (Table S1) with the exception of LPGGA-2 and HPPGA-6, for which pore/void spaces display diameters higher than 50 μm. Despite these structural differences, LPGGA-2, LPGGA-4 and HPPGA-6 showed adequate consistency and robustness (Figure 1e), holding PEDOT electrodes during electrochemical assays. In general, these three hydrogels exhibit dense plate- or leaf-like interconnected structures, giving place to dense and open macroporous networks. In contrast, the morphology of the rest of the hydrogels resembles that of microperforated polymeric films (Figure S4).[39] Accordingly, LPGGA-2, LPGGA-4 and HPPGA-6 hydrogels were chosen as suitable SE for OESC devices due to their mechanical stability and open structure.

Characterization of γ-PGA hydrogels

The FTIR spectra of *γ*-PGA, LPGGA-2, LPGGA-4 and HPPGA-6 are displayed in Figure S5. The spectrum recorded for *γ*-PGA shows the characteristic peaks expected for this biopolymer: C=O stretch of free carboxylic acid at 1728 cm^{-1}, stretching vibration of the amide carbonyl group (amide I) at 1638 cm^{-1}, asymmetric COO^- stretch at 1589 cm^{-1},–CONH– bond vibration (amide II) at 1535 cm^{-1} and C–N vibration at 1215 cm^{-1}. The disappearance of the free carboxylic acid and asymmetric COO^- bands and the significant enhancement of the amide I and II bands reflect the successful formation of –CONH– as cross-link bond (Scheme 1).

Thermogravimetric (TG and DTG) curves of the three selected hydrogels, after drying, are provided in Figure S6. Thermal behaviour was highly similar for the three samples. Specifically, TG curves clearly evidenced a small mass loss around 100 ºC that increases with the swelling capability of the hydrogel and, logically, corresponds to the

evaporation of still absorbed water. The three hydrogels were thermally stable, being observed a highly complex decomposition process at temperatures higher than 200 ºC. Note that DTG curves show different well-defined peaks that slightly changed with composition. For example, the most intense DTG peak appears at higher temperatures for the LPGGA-2 sample characterized by a lower content of cystamine cross-links. All samples have a high char yield (20-29%) due to their aromatic content, being this yield higher for the less cross-linked sample (*i.e.* LPGGA-2 with a higher ratio of *γ*-PGA).

Selection of γ-PGA hydrogel as electrolyte

The electrochemical response of PEDOT in each one of the *γ*-PGA hydrogels characterized in the previous section (*i.e.* LPGGA-2, LPGGA-4 and HPPGA-6) was investigated by CV and GCD measurements (Figure 2). Results have been compared with those obtained for an OESC device using $NaHCO_3$ (0.5 M) as electrolytic medium (Figure S7).

Firstly, five consecutive redox cycles were recorded from 0.0 to 0.8 V at different scan rates to evaluate: *i)* the oxidation and reduction charges during the charge-discharge process (Q_{ox} and Q_{red}, respectively); *ii)* the electroactivity of PEDOT, which corresponds to the similarity between the cathodic and anodic areas in the voltammograms (*i.e.* ratio between the reduction and oxidation charges, Q_{red}/Q_{ox}); *iii)* the current density reached at the reversal potential (*i.e.* anodic current density, j_a), which indicates the amount of oxidized molecules during the charging step; and, most importantly, *iv)* the *SC* of the system.

Figure 2 shows the 5th cyclic voltammogram recorded for each of the three systems at different scan rates. As it can be seen, the PEDOT response using LPGGA-2 is comparable to that of LPGGA-4 (Figures 2a and 2c), displaying similar Q_{ox}, Q_{red} and j_a

values (Figures 3a and 3c), especially at high scan rates. On the contrary, the amount of stored charge and current density obtained when HPPGA-6 is used as SE (Figure 2e) is considerably smaller than those reached for LPGGA-2 and LPGGA-4. These features indicate that the higher cross-linking degree of the former biohydrogel induces an excessively compact morphology (Figure 1b), precluding the transport of dopant ions towards the electrode-electrolyte interface during the oxidation and reduction processes of PEDOT. Moreover, cyclic voltammograms recorded for LPGGA-2 and LPGGA-4 almost have an ideal rectangular shape for scan rates up to 100 mV/s, which reflects a good capacitive performance and low contact resistance. Interestingly, the electrochemical behaviour of PEDOT in $NaHCO_3$ 0.5 M (Figure S7) resembles very closely that exhibited by HPGGA-6. Finally, since the current density at the reversal and initial potential (*i.e.* anodic and cathodic current density, respectively) varies linearly with the scan rate for the three SE γ-PGA hydrogels and $NaHCO_3$ (Figure 3c), we can conclude that the electrochemical processes are not controlled by diffusion.

The coulombic efficiency was higher than 0.75 for all four electrolytes regardless the current density employed (Figure 3d). Finally, the *SC* values obtained from CV measurements are displayed in Figure 3e. For low scan rates (*i.e.* below 50 mV/s), *SC* values are higher when using any of the three γ-PGA hydrogels as electrolyte than $NaHCO_3$ (0.5 M). However, for scan rates from 75 to 200 mV/s, OESC systems based on LPGGA-2 and LPGGA-4 reveal considerably enhanced *SC* values in comparison to HPGGA-6 and $NaHCO_3$ (Table 1). A similar behaviour was also observed when OESC devices were tested using GCD measurements (Figure 3f and Table 2). In this case, charging-discharging processes of PEDOT at different current densities (Figure 2b, 2d and 2f) led to symmetric GCD curves with a typical triangular shape and a V_{drop} at the

beginning of the discharging. The voltage drop was around 0.03 V for both LPGGA-2 and LPGGA-4, increasing to 0.12 V for HPGGA-6.

Overall, the results described in this section denote both LPGGA-2 and LPGGA-4 as promising biohydrogel-based SE for supercapacitor applications. However, in order to select only one γ-PGA hydrogel composition, the capacitance response of PEDOT in each one of the three tested hydrogel compositions and $NaHCO_3$ (0.5 M) was plotted in a Ragone graph (Figure S8). This plot indicates the relation between the energy density (how much energy is available, vertical axis) and the power density (how quickly it can be delivered, horizontal axis).[40] The E_{max} and P_{max} (Eqs 6-8) values were calculated using the *SC* values obtained from GCD measurements (5^{th} cycle) at different current densities (Table S2). As it was stated by Stoller and Ruoff,[35] both E_{max} and P_{max} should be computed by considering the total mass of the device, which also includes electrochemically intert components and the electrolyte. However, in this specific case since the comparison is only within γ-PGA hydrogel systems, *m* only refers to the mass of one electrode (*i.e.* 0.4113 mg) and, therefore, the values summarized in Table S2 cannot be compared with those reported in other works that rigorously considered the mass of the whole compact OESC device.

Hence, considering that energy storage research focuses on moving the device performance towards higher E_{max} and P_{max} values (the upper-right corner of Ragone plots),[41] Figure S8 evidences that devices based on LPPGA-2 are the best option, closely followed by LPGGA-4. However, it is important to bear in mind that Ragone plots only take into consideration one feature of the OESCs performance, thus not evaluating other possible determining factors, such as maximum voltage, leakage current, equivalent series resistance (ESR), cycle lifetime, energy efficiency, self-discharging, cost, or processability factors (*i.e.* size, ease of preparation, and mechanical

robustness of the final device).[40] Consequently, with PEDOT as electrodes, LPGGA-4 is the most suitable hydrogel to perform as SE due to both the excellent supercapacitor response obtained (enhanced *SC* values) and the mechanical stability of the system. Brunauer–Emmett–Teller (BET) analyses of LPGGA-4 hydrogel reveal a surface area of 6.3±0.1 m^2/g, whereas that of PEDOT electrodes prepared using similar conditions was reported to be between 30 and 50 m^2/g.[25] Next sections are exclusively focused on further exploring the response of PEDOT/*γ*-PGA OESC devices using LPGGA-4 as electrolyte (*i.e.* PEDOT/LPGGA-4 OESC).

PEDOT/ LPGGA-4 as energy storage device

This section includes further characterization of the supercapacitor response of PEDOT/LPGGA-4 OESC devices regarding: (1) cyclability and long-term stability; (2) leakage-current (LC) and self-discharging (SD) response; and (3) practical application (LED bulb). However, before discussing these results, the system was analysed from another perspective. As mentioned above, the LPGGA-4 SE presents some components in excess since it was employed in OESC devices without applying a washing step (*i.e.* the excess EDC or cystamine was not removed). Therefore, it would be interesting to understand the influence of EDC, cystamine, and *γ*-PGA on the electrochemical response of PEDOT.

Figures 4a-4b compare the 5th CV and GCD cycles recorded at 50 mV/s and 1.22 A/g, respectively, of PEDOT-based OESC devices using as electrolyte the following five systems: *A)* control electrolyte (0.5 M $NaHCO_3$); *B)* as prepared LPGGA-4 hydrogel; *C)* LPGGA-4 washed in distillate water for 3 days; *D)* LPGGA-4 washed in distillate water for 3 days and immersed in 0.5 M $NaHCO_3$ for 24 h; and *E)* LPGGA-4 lyophilized and subsequently immersed in 0.5 M $NaHCO_3$ for 24 h. The *SC* values

obtained from such measurements are summarized in Table S3. Comparison of the results obtained for the as prepared and washed LPGGA-4 hydrogels (*B* and *C*, respectively) indicates that the elimination of non-covalently linked species, EDC and $NaHCO_3$, causes a drastic reduction of the *SC* values (*i.e.* from 131.8 / 158.8 F/g to 22 / 881 F/g determined using CV / GDC curves, respectively). Systems *D)* and *E)*, which were designed to re-absorb the $NaHCO_3$ dopant after it was washed out, did not result in higher *SC* values. Overall, results reflect that the $NaHCO_3$ dopant ions coming from synthesis of the hydrogel must be preserved by avoiding the washing step, since its re-absorption is not easy task.

Regarding the influence of EDC, cystamine, and γ-PGA, Figures S9a-b show the 5^{th} CV and GCD cycles recorded at 50 mV/s and 1.22 A/g, respectively, of PEDOT-based OESC devices using as electrolyte the following three additional systems: *F)* low M_w γ-PGA (0.5 M) in $NaHCO_3$ (0.5 M), *G)* EDC (0.5 M) in $NaHCO_3$ (0.5 M); and *H)* cystamine (0.25 M) in $NaHCO_3$ (0.5 M). The *SC* values obtained from such measurements, which are summarized in Table S3, were higher than that of the control electrolyte *A*) and very similar to that of the as prepared LPGGA-4 *B*), especially for *F*) and *G*) electrolytic media. These results indicate that the presence of both EDC and γ-PGA in the electrolyte enhances the electrochemical response of OESC device.

As highlighted by McCloskey,[41] it seems of major importance to identify new electrode and electrolyte materials for obtaining enhanced *SC* and, in turn, higher energy density, by better understanding electrode−electrolyte interactions. Although this consideration is beyond the scope of the current study, theoretical molecular dynamics calculations are a good strategy to fulfil such goal by guiding the OESC optimization performance.[42,43]

Cyclability and long-term stability

PEDOT/LPGGA-4 OESC devices were submitted to thousands of cycles to determine their cyclability, which is an important factor when considering a supercapacitor adequate for practical applications (Figure 5 and Table 3). Specifically, PEDOT/LPGGA-4 OESCs were submitted to one-thousand consecutive CV cycles from 0 to 0.8 V at a scan rate of 50 mV/s (Figure 5a). After such amount of cycles, the *SC* decrease from 161 F/g (5^{th} cycle) to 136 F/g, which represents 84% of *SC* retention. During oxidation and reduction processes, swelling and shrinkage phenomena derived from consecutive doping–dedoping steps induce structural changes in PEDOT electrodes. Hence, once the equilibrium is reached, the final morphology is more compact and, therefore, the access and escape of dopant ions is reduced in comparison to the first stages of PEDOT response. This explains the reduction in *SC* values, as well as the LEA value, which is constant at *ca.* 17% after 1000 CV cycles (Figure 5b and Table 3). However, this response is more related to the electrode material rather than the electrolyte, which further confirms the suitability of LPGGA-4 as electrolytic medium.

Besides, PEDOT/LPGGA-4 OESC were also submitted to two-thousand consecutive GCD cycles from 0 to 0.8 V at a current density of 1.22 A/g (Figures 5c-5d and Table 3). GCD curves exhibited a typical triangular shape with a small voltage drop (*i.e.* 0.06 V) at the beginning of the discharging step. This drop is practically identical to that reported for OESCs prepared by combining PEDOT electrodes and κ-carrageenan hydrogels,[25] and similar to that achieved for devices fabricated using graphene/polypyrrole electrodes immersed in porous cellulose.[44] The symmetric charge-discharge curves indicate high coulombic efficiency and good reversibility, reflecting the excellent capacitive properties of PEDOT.[6,11,45] The latter is consistent with the high *SC* value obtained for the 2^{nd} charge-discharge cycle (168 F/g). After 2000 consecutive

GCD cycles, the *SC* decreased to 136 F/g, which corresponds to 81% of *SC* retention. Again, the structural changes in the morphology induced by the swelling and shrinkage of PEDOT during oxidation and reduction processes slightly reduce the *SC* of PEDOT/LPGGA-4 after 2000 consecutive GCD cycles. In addition, to examine the lifetime stability of PEDOT/LPGGA-4 OESCs, this galvanostatic assay was repeated to the devices one week later. Figures 5c and 5d compare the results obtained for as prepared OESC devices (t_0) with those obtained for devices examined one week after (t_{1w}), while numerical values are listed in Table 3. After one week, the *SC* of prepared devices decreased from 168 F/g to 148 F/g (2^{nd} cycle) at a constant current density of 1.22 A/g from 0.0 to 0.8 V, which represents a reduction of only 12%, and the voltage drop increases to 0.10 V. More interestingly, after 2000 GCD cycles, the *SC* value of as-prepared devices (136 F/g) resembles that of devices examined one week later (130 F/g). This small difference (4%) corroborates that the structure and morphology of PEDOT is completely stabilized after 2000 GCD cycles and stable for 7 days.

Leakage-current and self-discharging response

The LC corresponds to the stable parasitic current expected when the capacitor is held indefinitely on charge at the rated voltage,[36] while the SD is associated with the voltage drop of a charged capacitor after a set period of time and its effects on the power and energy densities.[46] Assays to evaluate both the LC and the SD response, which were run using three independent PEDOT/LPGGA-4 devices, were performed by charging the OESCs to 0.8 V at 0.25 mA. The LC was determined by keeping the potential at 0.8 V for 5 min and monitoring the current data through the device. Figure 6a displays that the current rapidly decreases to a minimum value of 51.3 μA, staying at that value for the remaining time. This small LC reflects the good stability of

PEDOT/LPGGA-4 devices. On the other hand, the SD response was evaluated by keeping the charged device at 1×10^{-11} mA for 10 min (self-discharge) and, after this period of time, the device was discharged to 0.0 V at –1 mA. Figure 6b reveals that in all cases the voltage of the device ends above 0.45 V after the period of time set for self-discharge. Additional SD experiments keeping the charge for 2 hours corroborated the low self-discharge tendency of the device (Figure S10), the voltage being 0.41 V after such period. Such response combined with the small LC corroborates the potential interest of PEDOT/LPGGA-4 OESC devices for practical applications.

Practical application (LED bulb)

In order to show the potential application of PEDOT/LPGGA-4 OESC devices, four units, as the one depicted in Figure S1b, were connected in series and used to power a red LED bulb (lowest working potential = 1.65-1.7 V). The preparation process of the tandem device is illustrated in Figure S11. When connecting four identical capacitors in series, each voltage threshold V and capacitance C is combined to theoretically result in a voltage threshold equal to $4V$ and a capacitance of $1/4C$. Nevertheless, combining capacitors in series also leads to a higher ESR value, and slightly different LCs may induce voltage across each one to differ, thus leading to a resulting voltage threshold lower than the theoretical value.

Before powering the LED, the assembled device was characterized by 25 GCD cycles at 2 mA (charging and discharging times equal to 60 seconds). Figure 7a-b shows the stability of the system, which reaches the same final potential after such amount of cycles. Besides, the SD response of the system was also determined through the following procedure: the device was charged to 3 V at 2 mA, hold at 0 mA for 5 or 10 min (self-discharge), and, after time, the device was discharged to 0 V at -4 mA. This

procedure was repeated five times to ensure data reproducibility. Figure 7c reveals the low SD tendency of the four PEDOT/ LPGGA-4 OESC devices connected in series: the voltage ends above 1 V after ten minutes.

Finally, the assembled device was used to power a red LED bulb. Figure S12 shows the connections during the charging of the system to 3 V at 2 mA (charging time, t_c = 30") as well as during discharging (*i.e.* red LED bulb ON; Figure 7d). Briefly, during charging, **1** connects the four OESC units in series to the CE/RE, while **2** closes the circuit by connecting them to the WE/S electrode. Once the system is charged, connection **3** between the LED and the tandem device is established, and **1** and **2** are disconnected. The charging/discharging operation was successfully repeated several consecutive times (more than 15), being the red LED ON for 28.3 ± 1.0 seconds even though it was dimly lit even after 38 seconds (Figure S13). A representative video of the process can be found as ESI material.

CONCLUSIONS

In summary, we have selected the experimental conditions required to obtain γ-PGA hydrogels with *(i)* an open internal structure that facilitates the ion diffusion process through dense macroporous networks, and *(ii)* stable mechanical robustness to hold the electrodes, which ensures their use as SE in PEDOT/γ-PGA OESC devices. Although three hydrogels with pore size ranging from 19 to > 50 μm and SR varying between 140 and 1800% fulfilled such conditions, the one (LPGGA-4) with the smallest macropores (19.1 ± 7.7 μm) and intermediate SR (450%) induced the best response of PEDOT electrodes. The electrochemical performance of PEDOT/LPGGA-4 system is significantly higher than that of PEDOT/$NaHCO_3$(aq) devices used as a control. Additionally, the utilization of LPGGA-4 as SE provides good capacitor response and

cycling stability, small LC and SD tendency without water loss or evaporation. This work demonstrates the advances that can be achieved by selecting suitable biopolymeric hydrogel formulations as SEs, and their substantial potential for other energy devices design. Thus, the selected γ-PGA hydrogel not only maintains the excellent electrochemical response of PEDOT electrodes, but also provides sustainability, a light-weight solid support for the electrodes, and a porous structure that provides effective ion and electron transport.

SUPPORTING INFORMATION

Synthetic methods and characterization techniques. Figures S1-S13 and Tables S1-S3 as described in the text. This material is available free of charge via the internet at http://pubs.acs.org**.**

ACKNOWLEDGEMENTS

This work was supported by MINECO-FEDER (MAT2015-69367-R and MAT2015-69547-R). Support for the research of C.A. was received through the prize "ICREA Academia" for excellence in research funded by the Generalitat de Catalunya. Authors are thanked to Dr. R. Álvarez (UB) by his comments and suggestions.

REFERENCES

(1) Pandolfo A. G.; Hollenkamp, A. F. Carbon Properties and Their Role in Supercapacitors. *J. Power Sources* **2006**, *157*, 11–27.

(2) González, A.; Goikolea, E.; Barrena, J. A.; Mysyk, R. Review on Supercapacitors: Technologies and Materials. *Renew. Sustain. Energy Rev.* **2016**, *58*, 1189–1206.

(3) Yu, A.; Chabot, V.; Zhang, J. "Fundamentals of Electrochemical Pseudocapacitors," in *Electrochemical Supercapacitors for Energy Storage and Delivery: Fundamentals and Applications*, USA: CRC Press, Boca Raton, 2013, pp. 99–134.

(4) Patra, S.; Munichandraiah, N. Supercapacitor Studies of Electrochemically Deposited PEDOT on Stainless Steel Substrate. *J. Appl. Polym. Sci.* **2007**, *106*, 1160–1171.

(5) Liu, R.; Lee, S. B. MnO2/Poly(3,4-ethylenedioxythiophene) Coaxial Nanowires by One-Step Coelectrodeposition for Electrochemical Energy Storage. *J. Am. Chem. Soc.* **2008**, *130*, 2942–2943.

(6) Aradilla, D.; Azambuja, D.; Estrany, F.; Casas, M. T.; Ferreira, C. A.; Alemán, C. Hybrid Plythiophene–Clay Exfoliated Nanocomposites for Ultracapacitor Devices. *J. Mater. Chem.* **2012**, *22*, 13110–13122.

(7) Aradilla, D.; Estrany, F.; Casellas, F.; Iribarren, J.; Alemán, C. All-Polythiophene Rechargeable Batteries. *Org. Electr.* **2014**, *15*, 40–46.

(8) Xuan, Y.; Sandberg, M.; Crispin, X. An All-Polymer-Air PEDOT Battery. *Org. Electr.* **2012**, *13*, 632–637.

(9) Marzocchi, M.; Gualandi, I.; Calienni, M.; Zironi, I.; Scavetta, E.; Castellani, G.; Fraboni, B. Physical and Electrochemical Properties of PEDOT:PSS as a Tool for Controlling Cell Growth. *ACS Appl. Mater. Interfaces* **2015**, *7*, 17993–18003.

(10) del Valle, L. J.; Estrany, F.; Armelin, E.; Oliver, R.; Alemán, C. Cellular Adhesion, Proliferation and Viability on Conducting Polymer Substrates. *Macromol. Biosci.* **2008**, *8*. 1144–1151.

(11) Shi, Y.; Peng, L.; Yu, G. Nanostructured Conducting Polymer Hydrogels for Energy Storage Applications. *Nanoscale* **2015**, *7*, 12796–12806.

(12) Kirchmeyer, S.; Reuter, R. Scientific Importance, Properties and Growing Applications of Poly(3,4-ethylenedioxythiophene). *J. Mater. Chem.* **2005**, *15*, 2077–2088.

(13) Cho, S.; Shin, K.-H.; Jang, J. Enhanced Electrochemical Performance of Highly Porous Supercapacitor Electrodes Based on Solution Processed Polyaniline Thin Films. *ACS Appl. Mater. Interfaces* **2013**, *5*, 9186–9193.

(14) Xu, H.; Li, X.; Wang, G. Polyaniline Nanofibers with a High Specific Surface Area and an Improved Pore Structure for Supercapacitors. *J. Power Sources* **2015**, *294*, 16–21.

(15) Yan, L.; Rui, X.; Chen, G.; Xu, W.; Zou, G.; Luo, H. Recent Advances in Nanostructured Nb-Based Oxides for Electrochemical Energy Storage. *Nanoscale* **2016**, *8*, 8443–8465.

(16) Pan, L.; Yu, G.; Zhai, D.; Lee, H. R.; Zhao, W.; Liu, N.; Wang, H.; Tee, B. C.-K.; Shi, Y.; Cui, Y.; Bao, Z. Hierarchical Nanostructured Conducting Polymer Hydrogel with High Electrochemical Activity. *Proc. Natl. Acad. Sci.* **2012**, *109*, 9287–9292.

(17) Hu, X.; Xiong, W.; Wang, W.; Qin, S.; Cheng, H.; Zeng, Y.; Wang, B.; Zhu, Z. Hierarchical Manganese Dioxide/Poly(3,4-ethylenedioxythiophene) Core–Shell Nanoflakes on Ramie-Derived Carbon Fiber for High-Performance Flexible All-Solid-State Supercapacitor. *ACS Sustain. Chem. Eng.* **2016**, *4*, 1201–1211.

(18) Shao, L.; Jeon, J.-W.; Lutkenhaus, J. L. Porous Polyaniline Nanofiber/Vanadium Pentoxide Layer-by-Layer Electrodes for Energy Storage. *J. Mater. Chem. A*, **2013**, *1*, 7648–7656.

(19) Dettlaff A.; Wilamowska, M. Electrochemical Synthesis and Characterization of Nanocomposites Based on Poly(3,4-ethylenedioxythiophene) and Functionalized

Carbon Nanotubes. *Synth. Met.* **2016**, *212*, 31–43.

(20) Nabilah Azman, N. H.; Lim, H. N.; Sulaiman, Y. Effect of Electropolymerization Potential on the Preparation of PEDOT/Graphene Oxide Hybrid Material for Supercapacitor Application. *Electrochim. Acta* **2016**, *188*, 785–792.

(21) Ajjan, F. N.; Casado, N.; Rębiś, T.; Elfwing, A.; Solin, N.; Mecerreyes, D.; Inganäs, O. High Performance PEDOT/Lignin Biopolymer Composites for Electrochemical Supercapacitors. *J. Mater. Chem. A* **2016**, *4*, 1838–1847.

(22) Mike, J. F.; Lutkenhaus, J. L. Electrochemically Active Polymers for Electrochemical Energy Storage: Opportunities and Challenges**.** *ACS Macro Lett.* **2013**, *2*, 839-844.

(23) Pandey, G. P.; Rastogi, A. C.; Westgate, C. R. All-Solid-State Supercapacitors with Poly(3,4-ethylenedioxythiophene)-Coated Carbon Fiber Paper Electrodes and Ionic Liquid Gel Polymer Electrolyte. *J. Power Sources.* **2014**, *245*, 857–865.

(24) Liu, K.; Hu, Z.; Xue, R.; Zhang, J.; Zhu, J. Electropolymerization of High Stable Poly(3,4-ethylenedioxythiophene) and Its Applications in Electrochemical Capacitor. *J. Power Sources* **2008**, *179*, 8580–862.

(25) Pérez-Madrigal, M. M.; Estrany, F.; Armelin, E.; Díaz, D. D.; Alemán, C. Towards Sustainable Solid-State Supercapacitors: Electroactive Conducting Polymers Combined with Biohydrogels**.** *J. Mater. Chem. A* **2016**, *4*, 1792–1805.

(25) Zhao, C.; Zheng, W. A Review for Aqueous Electrochemical Supercapacitors. *Front. Energy Res.* **2015**, *3*, 1–11.

(27) Choudhury, N. A.; Sampath, S.; Shukla, A. K. Hydrogel-Polymer Electrolytes for Electrochemical Capacitors: An Overview. *Energy Environ. Sci.*, 2009, **2**, 55–67.

(28) Armelin, E.; Pérez-Madrigal, M. M.; Alemán, C.; Díaz, D. D. Current Status and Challenges of Biohydrogels for Applications as Supercapacitors and Secondary

Batteries. *J. Mater. Chem. A* **2016**, *4*, 8952–8968.

(29) Thome, C. B.; Gómez, C. G.; Noyes, H. E.; Housewright, R. D. Production of Glutamyl Polypeptide by *Bacillus Subtilis*. *J. Bacteriol.* **1954**, *68*, 307–315.

(30) Ashiuchi, M.; Kamei, T.; Baek, D. H.; Shin, S. Y.; Sung, M. H.; Soda, K.; Yagi, T.; Misono, H. Isolation of *Bacillus Subtilis* (*Chungkookjang*), a Poly-γ-glutamate Producer with High Genetic Competence. *Appl. Microbiol. Biotechnol.* **2001**, *57*, 764–769.

(31) Ogunleye, A.; Bhat, A.; Irorere, V. U.; Hill, D.; Williams, C.; Radecka, I. Poly-γ-Glutamic Acid: Production, Properties and Applications. *Microbiology* **2015**, *161*, 1–17.

(32) Matsusaki, M.; Serizawa, T.; Kishida, A.; Akashi, M. Novel Functional Biodegradable Polymer III: The Construction of Poly(γ-glutamic acid)-Sulfonate Hydrogel with Fibroblast Growth Factor-2 Activity. *J. Biomed. Mater. Res. Part A* **2005**, *73*, 485–491.

(33) Murakami, S.; Aoki, N. Bio-Based Hydrogels Prepared by Cross-Linking of Microbial Poly(γ-glutamic acid) with Various Saccharides. *Biomacromolecules* **2006**, *7*, 2122–2127.

(34) Taniguchi, M.; Kato, K.; Shimauchi, A.; Xu, P.; Fujita, K.-I.; Tanaka, T.; Tarui, Y.; Hirasawa, E. Physicochemical Properties of Cross-Linked Poly-gamma-glutamic Acid and Its Flocculating Activity Against Kaolin Suspension. *J. Biosci. Bioeng.* **2005**, *99*, 130–135.

(35) Stoller, M. D; Ruoff, R. S. Best Practice Methods for Determining an Electrode Material's Performance for Ultracapacitors. *Energy Environ. Sci.* **2010**, *3*, 1294–1301.

(36) Xu, Y.; Lin, Z.; Huang, X.; Liu, Y.; Huang, Y.; Duan, X. Flexible Solid-State

Supercapacitors Based on Three-Dimensional Graphene Hydrogel Films. *ACS Nano* **2013**, *7*, 4042–4049.

(37) Yu, A.; Chabot, V.; Zhang, J. "Characterization and Diagnosis Techniques for Electrochemical Supercapacitors," in *Electrochemical Supercapacitors for Energy Storage and Delivery: Fundamentals and Applications*, USA: CRC Press, Boca Raton, 2013, pp. 277–316.

(38) Matsusaki, M.; Yoshida, H.; Akashi, M. The Construction of 3D-Engineered Tissues Composed of Cells and Extracellular Matrices by Hydrogel Template Approach. *Biomaterials* **2007**, *28*, 2729–2737.

(39) Puiggalí-Jou, A.; Medina, J.; del Valle, L. J.; Alemán, C. Nanoperforations in Poly(lactic acid) Free-Standing Nanomembranes to Promote Interactions with Cell Filopodia. *Eur. Polym. J.* **2016**, *75*, 552–564.

(40) Gogotsi, Y.; Simon, P. True Performance Metrics in Electrochemical Energy Storage. *Science* **2011**, *334*, 917–918.

(41) McCloskey, B. D. Expanding the Ragone Plot: Pushing the Limits of Energy Storage. *J. Phys. Chem. Lett.* **2015**, *6*, 3592–3593.

(42) Jiang, D.; Wu, J. Microscopic Insights into the Electrochemical Behavior of Nonaqueous Electrolytes in Electric Double-Layer Capacitors. *J. Phys. Chem. Lett.* **2013**, *4*, 1260–1267.

(43) Lian, C.; Jiang, D.; Liu, H.; Wu, J. A Generic Model for Electric Double Layers in Porous Electrodes. *J. Phys. Chem. C* **2016**, *120*, 8704–8710.

(44) De Adhikari, A.; Oraon, R.; Tiwari, S. K.; Lee, J. H.; Nayak, G. C. Effect of Waste Cellulose Fibres on the Charge Storage Capacity of Polypyrrole and Graphene/Polypyrrole Electrodes for Supercapacitor Application. *RSC Adv.* **2015**, *5*, 27347–27355

(44) Aradilla, D.; Estrany, F.; Alemán, C. Symmetric Supercapacitors Based on Multilayers of Conducting Polymers. *J. Phys. Chem. C* **2011**, *115*, 8430–8438.

(45) Andreas, H. A. Self-Discharge in Electrochemical Capacitors: A Perspective Article. *J. Electrochem. Soc.* **2015**, *162*, A5047–A5053.

CAPTIONS TO FIGURES

Figure 1. Morphology of freeze-dried γ-PGA hydrogels: SEM images of (a) LPGGA-2; (b) HPGGA-6; and (c-d) LPGGA-4. Image (d) corresponds to a magnified area from (c). (e) Optical images of the studied hydrogels. (f) Pore size relative frequency of LPGGA-4.

Figure 2. Electrochemical characterization of PEDOT/γ-PGA OESCs (two-electrode configuration, CE/RE=WE/S = PEDOT) using (a-b) LPGGA-2, (c-d) LPGGA-4 and (e-f) HPGGA-6 as SE. (a, c, e) Cyclic voltammograms (5^{th} cycle shown) recorded from 0 to 0.8 V at scan rates of 10, 25, 50, 75, 100, 150 and 200 mV/s. (b, d, f) GCD curves recorded from 0 to 0.8 V at different current densities (A/g). Solid lines correspond to the second charge-discharge cycle, while the dashed ones correspond to the fifth cycle.

Figure 3. Electrochemical characterization of PEDOT/γ-PGA OESC devices (two-electrode configuration, CE/RE=WE/S = PEDOT) using different electrolyte media. (a) Variation of the stored charge (Q_{ox}); (b) electrochemical activity defined as Q_{red}/Q_{ox}; (c) current density *versus* scan rate. The anodic intensity at reversal potential (*i.e.* 0.8 V) and cathodic intensity at 0.1 V were taken from the cyclic voltammograms displayed in Figure 2; (d) coulombic efficiency of GCD curves displayed in Figure 2; (e-f) specific capacitance values obtained from (e) CV and (f) GCD measurements (Figure 2).

Figure 4. Electrochemical characterization of PEDOT-based OESC devices (two-electrode configuration, CE/RE=WE/S = PEDOT) using five different electrolytic systems: *(A)* control electrolyte (0.5 M $NaHCO_3$); *(B)* as prepared LPGGA-4 hydrogel; *(C)* LPGGA-4 washed in distillate water for 3 days; *(D)* washed-LPGGA-4 in 0.5 M $NaHCO_3$ for 24h; and *(E)* lyophilized-LPGGA-4 immersed in 0.5 M $NaHCO_3$ for 24h. For each system both the (a) cyclic voltammogram recorded from 0 to 0.8 V at 50 mV/s

and (b) GCD curve recorded from 0 to 0.8 V at 1.22 A/g are displayed (5^{th} cycle shown in both cases).

Figure 5. Cycling stability of PEDOT/LPGGA-4 OESC devices (two-electrode configuration, CE/RE=WE/S = PEDOT): (a) Cyclic voltammograms from 0 to 0.8 V at 50 mV/s; (b) *SC* and LEA values calculated with data derived from (a); (c) GCD curves recorded from 0 to 0.8 V at 1.22 A/g for devices tested just as prepared (t_0) and after one week of their preparation (t_{1w}). Solid lines correspond to the second cycle, while dashed one correspond to the 2000^{th} cycle; (d) *SC* values calculated with data derived from (c).

Figure 6. (a) Leakage current and (b) self-discharge curves for PEDOT/LPGGA-4 OESC devices.

Figure 7. Four assembled PEDOT/LPGGA-4 OESC devices connected in series: (a) 25 GCD curves recorded at 2 mA ($t_c = t_d = 60$”); (b) 2^{nd} (solid line) and 25^{th} GCD cycle (dashed line) from (a); (c) self-discharge response of the tandem system; (d) red LED powered.

Table 1. Specific capacitance values (*SC*, in F/g) determined from cyclic voltammograms obtained for PEDOT/γ-PGA OESC and control devices using different scan rates (Figure 2 and Figure S7a).

Scan rate (mV/s)	**HPGGA-6**	**LPGGA-4**	**LPGGA-2**	**$NaHCO_3$ (0.5 M)**
10	90.5 ± 3.7	113.8 ± 4.0	134.8 ± 4.6	34.9 ± 13.2
25	87.3 ± 13.2	138.2 ± 3.9	155.2 ± 3.3	54.3 ± 11.8
50	71.4 ± 20.1	144.1 ± 4.1	154.6 ± 3.3	63.0 ± 10.4
75	58.1 ± 21.9	140.6 ± 4.3	145.3 ± 9.8	66.3 ± 9.0
100	44.3 ± 20.4	140.8 ± 11.6	142.9 ± 1.2	68.4 ± 7.5
150	37.7 ± 0.3	116.1 ± 6.0	110.4 ± 20.6	64.5 ± 7.9
200	27.7 ± 1.9	99.7 ± 6.8	91.4 ± 22.2	62.0 ± 6.3

Table 2. Specific capacitance values (*SC*, in F/g) determined from GCD curves obtained for PEDOT/γ-PGA OESC devices and control using different current densities (Figure 2 and Figure S7b).

Current Density (A/g)	**HPGGA-6**	**LPGGA-4**	**LPGGA-2**	**$NaHCO_3$ (0.5 M)**
		2nd Cycle		
0.30	83 ± 1			
0.44	84 ± 1	139 ± 8	157 ± 3	62 ± 6
0.61	86 ± 1	144 ± 6	157 ± 5	64 ± 7
1.22		149 ± 6	165 ± 10	65 ± 7
2.43		157 ± 6	172 ± 16	65 ± 7
4.86		158 ± 7	162 ± 13	66 ± 6
		5th Cycle		
0.30	83± 6			
0.44	87 ± 6	140 ± 8	159 ± 1	62 ± 7
0.61	87 ± 2	146 ± 6	159 ± 6	64 ± 7
1.22		149 ± 7	165 ± 10	64 ± 7
2.43		152 ± 5	171 ± 14	65 ± 7
4.86		158 ± 7	162 ± 12	66 ± 6

Table 3. Specific capacitance values (*SC*, in F/g), oxidation and reduction charges (Q_{ox} and Q_{red}, in mC/g), loss of electroactivity (LEA; in %), charging time (t_c; in s) and coulombic efficiency (η, in %) determined from CV and GCD curves obtained for PEDOT/LPGGA-4 OESC device s (Figure 6).

	***SC* (F/g)**	**Q_{ox} (mC/g)**	**Q_{red} (mC/g)**	**LEA (%)**
5th CV cycle	161.3	57.2	55.0	5.3
1000th CV cycle	135.8	49.4	49.0	16.9
	***SC* (F/g)**	**t_c (s)**	**η (%)**	
2nd GCD cycle (t_0)	167.7	62.7	88.2	
2000th GCD cycle (t_0)	136.3	48.0	87.9	
2nd GCD cycle (t_{1w})	147.9	38.4	94.3	
2000th GCD cycle (t_{1w})	129.8	41.8	93.8	

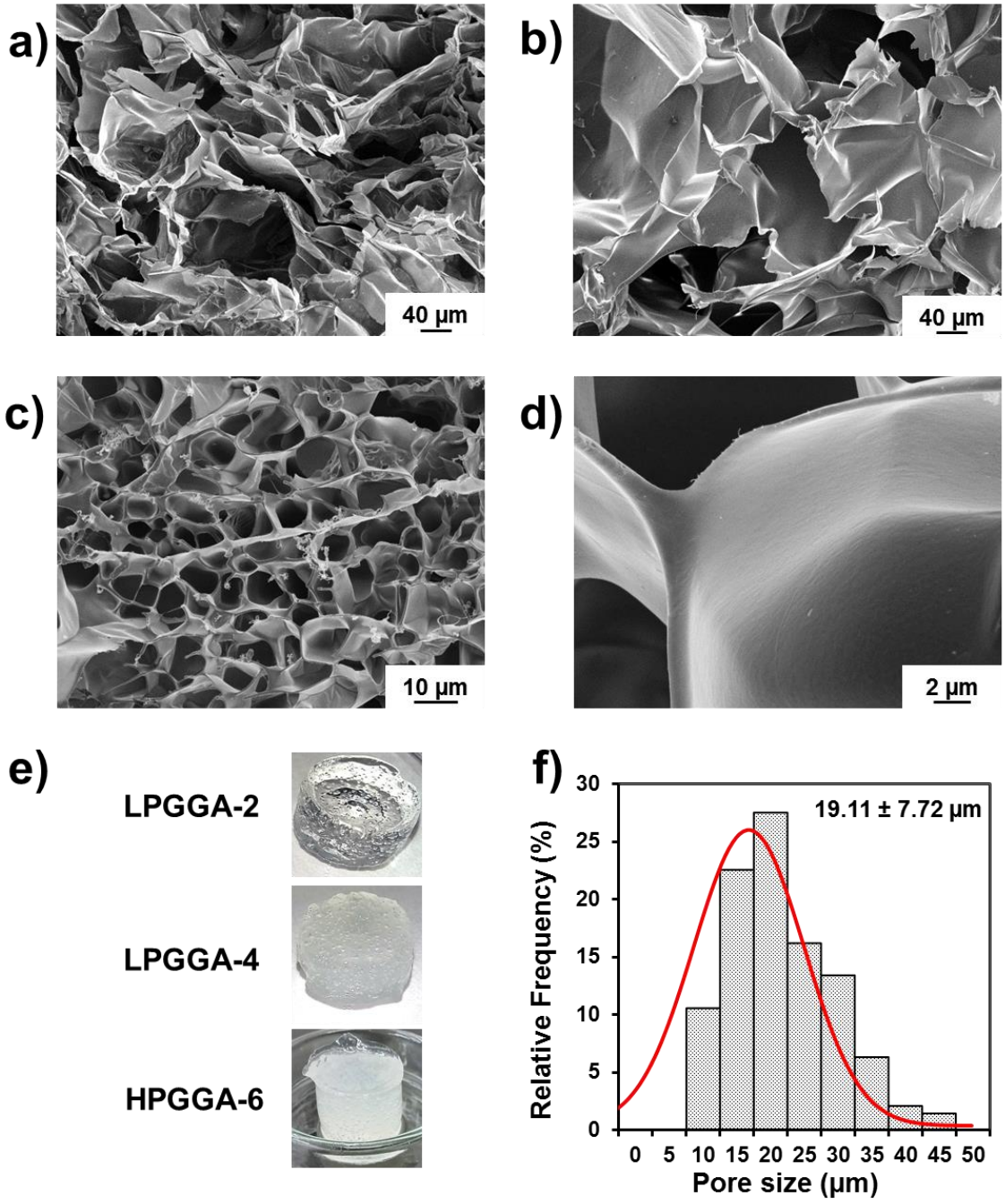
a)
40 µm
b)
40 µm
c)
10 µm
d)
2 µm
e)
LPGGA-2
LPGGA-4
HPGGA-6
f)
19.11 ± 7.72 µm
Relative Frequency (%)
0
5
10
15
20
25
30
0 5 10 15 20 25 30 35 40 45 50
Pore size (µm)

Figure 1

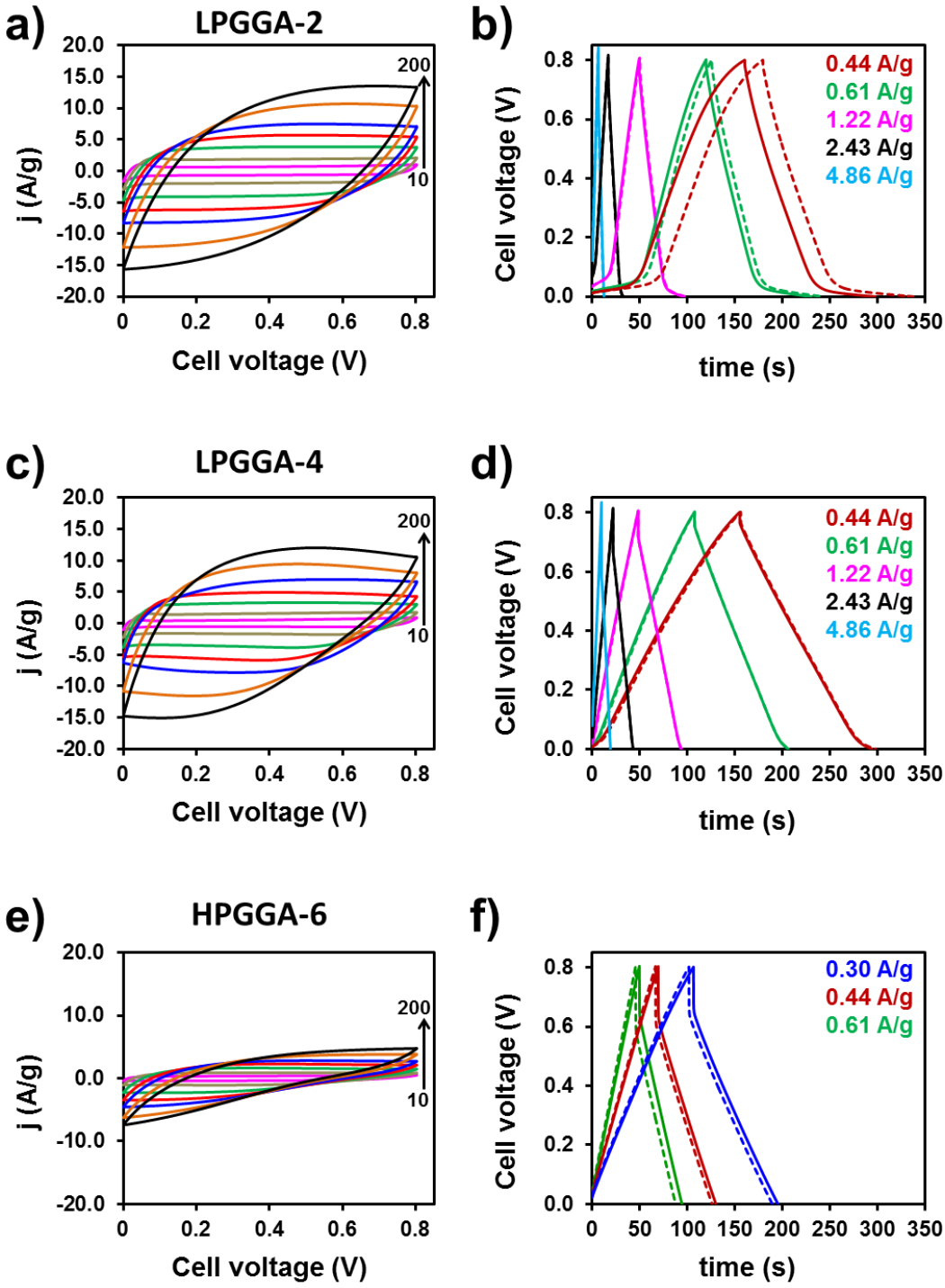
a)
LPGGA-2
j (A/g)
Cell voltage (V)
200
10
b)
Cell voltage (V)
time (s)
0.44 A/g
0.61 A/g
1.22 A/g
2.43 A/g
4.86 A/g
c)
LPGGA-4
d)
e)
HPGGA-6
f)
0.30 A/g
0.44 A/g
0.61 A/g

Figure 2

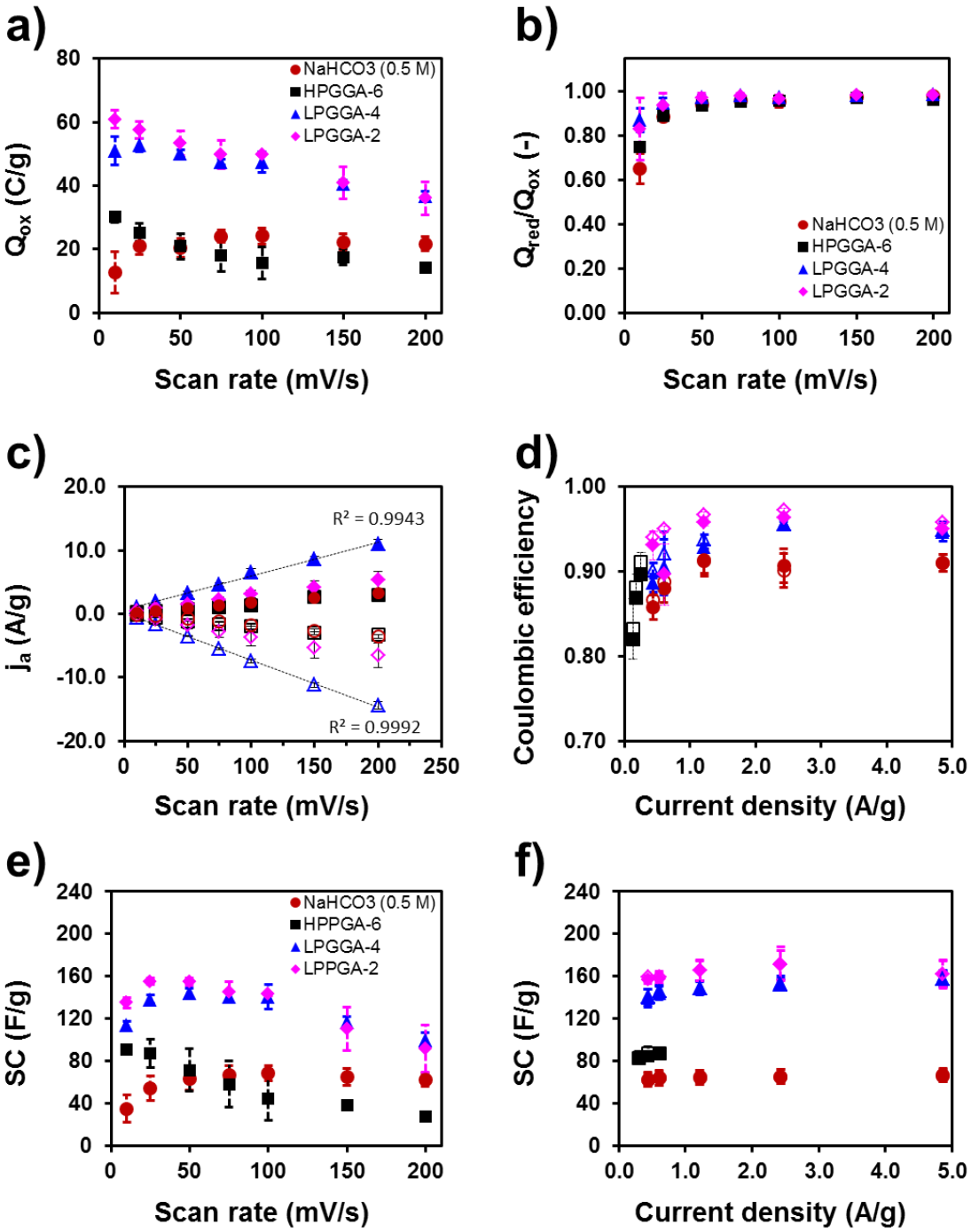
a)
Q_{ox} (C/g)
Scan rate (mV/s)
NaHCO3 (0.5 M)
HPGGA-6
LPGGA-4
LPGGA-2
b)
Q_{red}/Q_{ox} (-)
Scan rate (mV/s)
NaHCO3 (0.5 M)
HPGGA-6
LPGGA-4
LPGGA-2
c)
j_a (A/g)
Scan rate (mV/s)
R² = 0.9943
R² = 0.9992
d)
Coulombic efficiency
Current density (A/g)
e)
SC (F/g)
Scan rate (mV/s)
NaHCO3 (0.5 M)
HPPGA-6
LPGGA-4
LPPGA-2
f)
SC (F/g)
Current density (A/g)

Figure 3

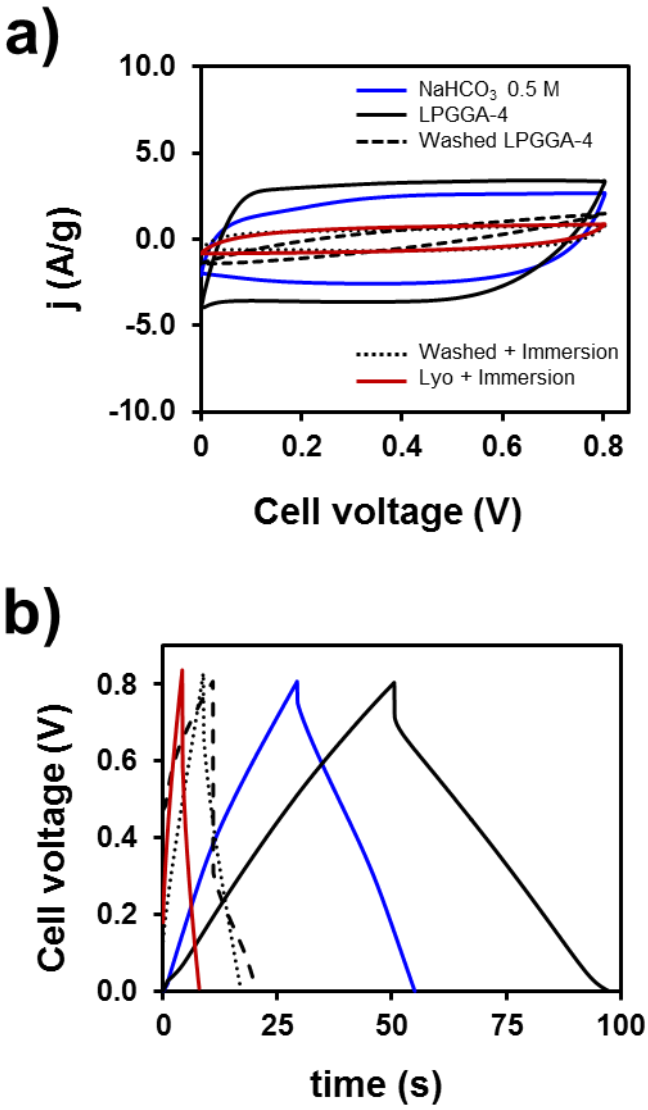
a)
10.0
5.0
0.0
-5.0
-10.0
j (A/g)
0
0.2
0.4
0.6
0.8
Cell voltage (V)
NaHCO3 0.5 M
LPGGA-4
Washed LPGGA-4
Washed + Immersion
Lyo + Immersion
b)
0.8
0.6
0.4
0.2
0.0
Cell voltage (V)
0
25
50
75
100
time (s)

Figure 4

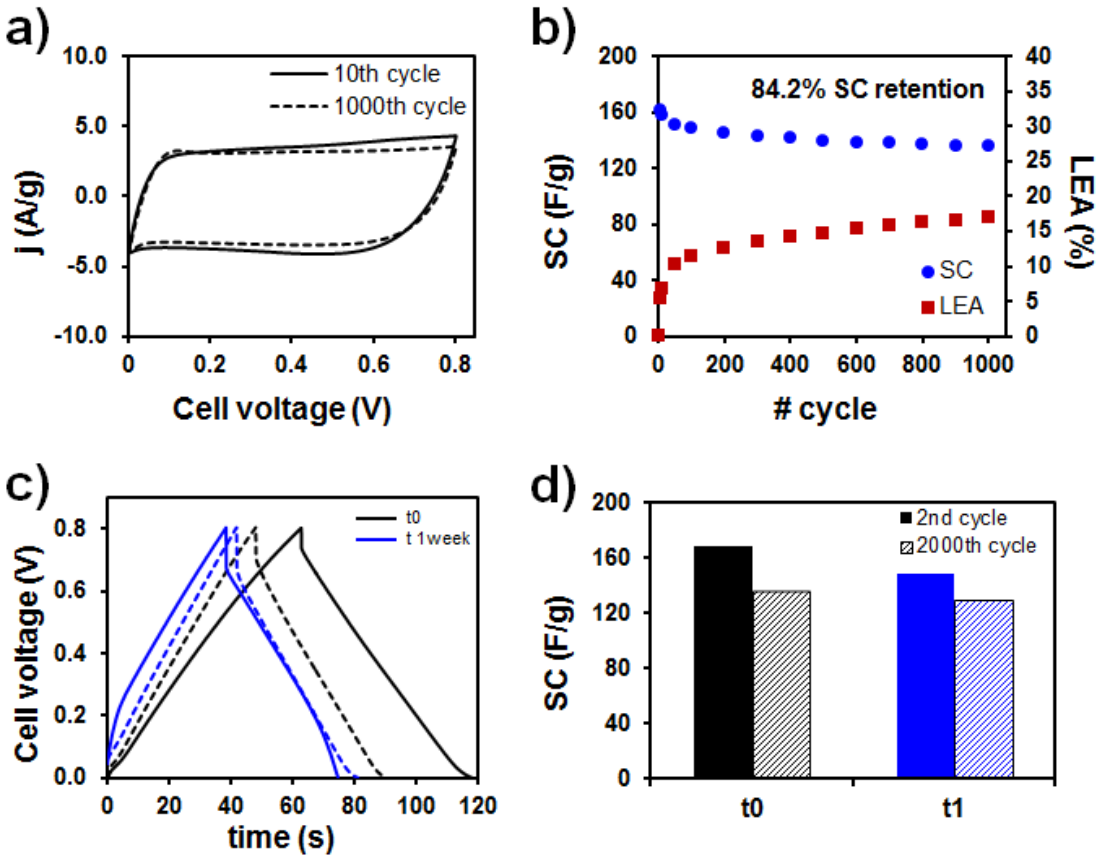
a)
10th cycle
1000th cycle
j (A/g)
Cell voltage (V)
b)
84.2% SC retention
SC
LEA
SC (F/g)
LEA (%)
cycle
c)
t0
t 1week
Cell voltage (V)
time (s)
d)
2nd cycle
2000th cycle
SC (F/g)
t0
t1

Figure 5

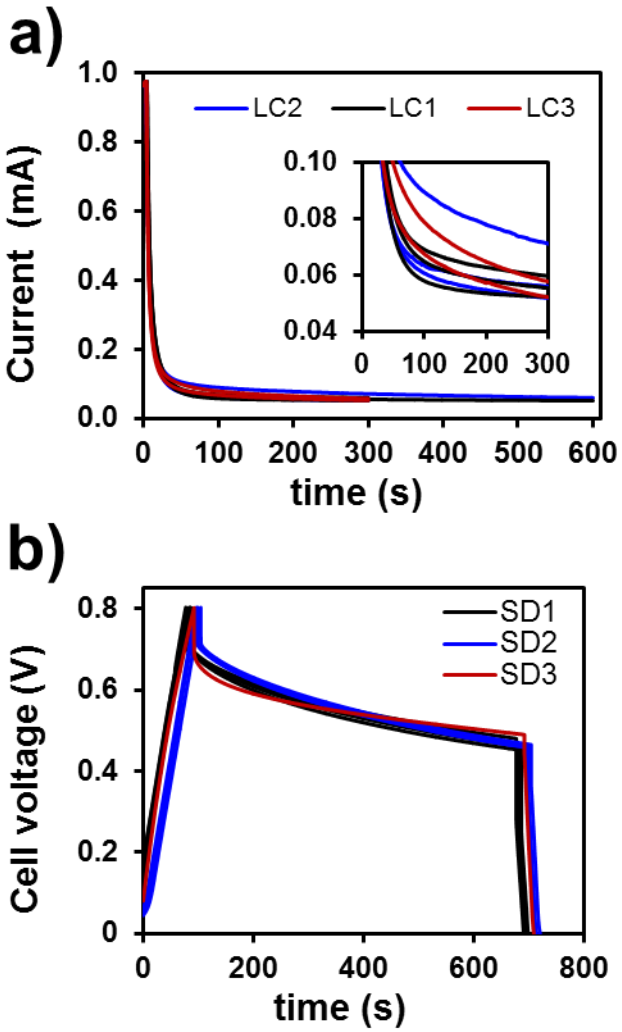
a)
1.0
0.8
0.6
0.4
0.2
0.0
Current (mA)
LC2
LC1
LC3
0.10
0.08
0.06
0.04
0
100
200
300
0
100
200
300
400
500
600
time (s)
b)
0.8
0.6
0.4
0.2
0
Cell voltage (V)
SD1
SD2
SD3
0
200
400
600
800
time (s)

Figure 6

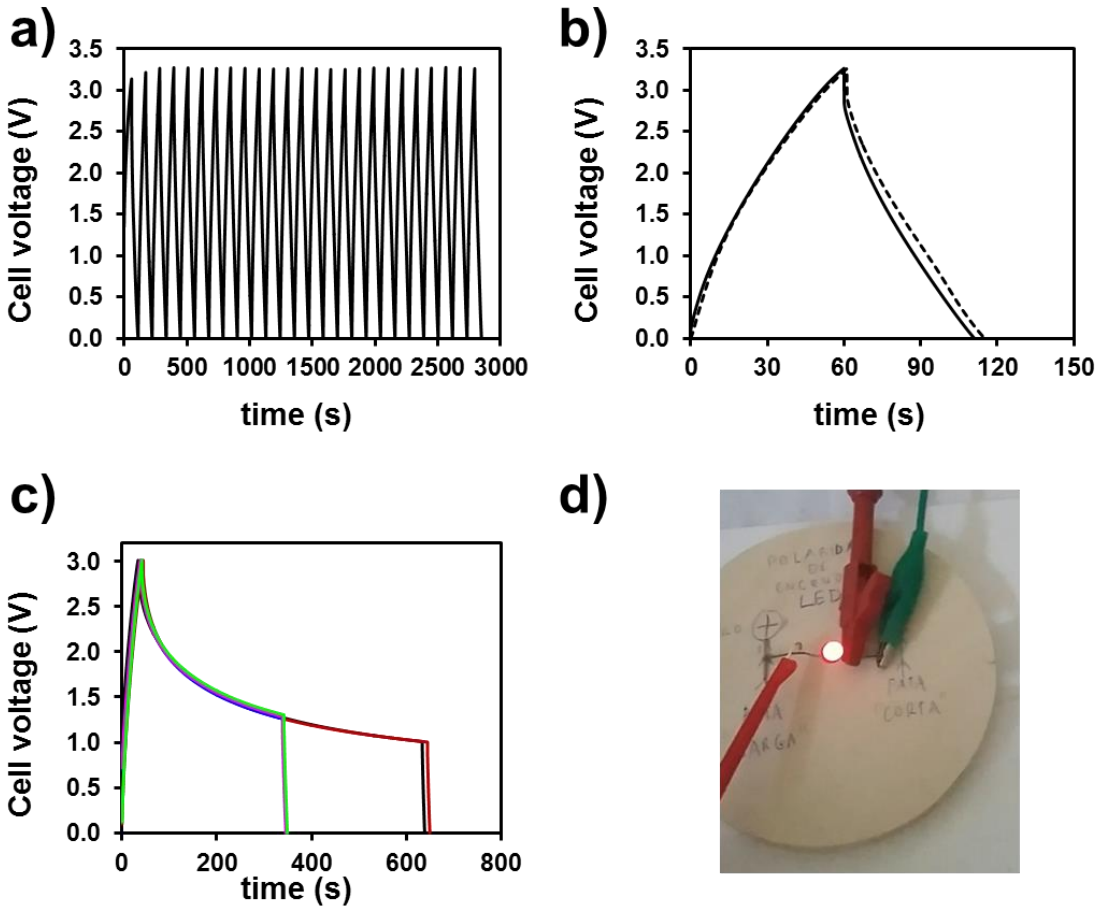
a)
Cell voltage (V)
3.5
3.0
2.5
2.0
1.5
1.0
0.5
0.0
0
500
1000
1500
2000
2500
3000
time (s)
b)
Cell voltage (V)
3.5
3.0
2.5
2.0
1.5
1.0
0.5
0.0
0
30
60
90
120
150
time (s)
c)
Cell voltage (V)
3.0
2.5
2.0
1.5
1.0
0.5
0.0
0
200
400
600
800
time (s)
d)

Figure 7

TOC Graphic